High and asymmetric somato-dendritic coupling of V1 layer 5 neurons independent of behavioural state and visual stimulation

Valerio Francioni[1,2] and Nathalie L. Rochefort[1,2,†]

[1]Centre for Discovery Brain Sciences, School of Biomedical Sciences Edinburgh, Edinburgh, EH8 9XD, United Kingdom.

[2]Simons Initiative for the Developing Brain, University of Edinburgh, Edinburgh, EH8 9XD, United Kingdom.

[†] Corresponding Author:
Nathalie Rochefort
Centre for Discovery Brain Sciences, Biomedical Sciences Edinburgh, Edinburgh, EH8 9XD, United Kingdom.
n.rochefort@ed.ac.uk

Abstract

Active dendritic conductances impact the integration of synaptic inputs. However, the extent to which dendrites act as independent computational subunits *in vivo*, remains unclear. We imaged semi-simultaneously calcium signals in the soma, trunk and distal tuft dendrites of individual layer 5 pyramidal neurons in the awake primary visual cortex. We found highly correlated calcium transients throughout the whole apical tuft: branch-specific activity was rare and limited to the smallest calcium transients. While apical tuft calcium transients were highly correlated to trunk and somatic transients, the frequency of calcium transients was found to decrease in a distance- and amplitude-dependent manner from soma to apical tuft. Visual stimulation and locomotion increased global apical tuft activity but did not alter the coupling between soma and apical tuft. These results suggest that the apical tuft acts as a single computational unit and that its coupling to somatic signals is strong and asymmetric.

Introduction

Cortical layer 5 excitatory neurons are characterized by long apical dendrites receiving inputs from multiple long-range cortical and subcortical connections (Harris and Shepherd, 2015; Ramaswamy and Markram, 2015). In the primary visual cortex (V1), layer 5 pyramidal neurons display selective responses to physical features of visual stimuli, such as the orientation and direction of movement (Kim *et al.*, 2015). In addition, layer 5 neurons activity is modulated by locomotion both in darkness and during visual stimulation (Erisken *et al.*, 2014; Dadarlat and Stryker, 2017; Dipoppa *et al.*, 2018), suggesting that V1 layer 5 neurons integrate inputs from anatomically and functionally distinct pathways (visual and motor-related). However, the integration of visual and locomotion-related inputs and its relationship with somatic output remains unknown.

Dendritic properties were shown to support both distance-dependent filtering and local dendritic non linearities (Grienberger, Chen and Konnerth, 2015; Stuart and Spruston, 2015). Different types of active dendritic currents have been described to support local nonlinear events, primarily driven by NMDA-receptors calcium and sodium- conductances both *in vitro* and *in vivo* (Schiller *et al.*, 1997; Matthew E. Larkum, Zhu and Sakmann, 1999, for review, Grienberger, Chen and Konnerth, 2015; Stuart and Spruston, 2015). These dendritic events are generally associated with calcium influx both locally and globally in the apical tuft of layer 5 neurons (Xu *et al.*, 2012; Hill *et al.*, 2013; Palmer *et al.*, 2014; Cichon and Gan, 2015; Manita *et al.*, 2015; Takahashi *et al.*, 2016). Additionally, the coincident occurrence of back-propagating action potentials and tuft depolarization was shown to generate widespread calcium transients in the apical tuft dendrites (Jaffe *et al.*, 1992; Spruston *et al.*, 1995; Magee and Johnston, 1997; Svoboda *et al.*, 1997; Helmchen *et al.*, 1999; Larkum, Zhu and Sakmann, 1999; Waters *et al.*, 2003; Manita *et al.*, 2015) .

The frequency and dynamics of local dendritic nonlinearities *in vivo* have been a matter of debate. In the motor cortex, one study suggested that individual branches of densely labelled layer 5 neurons selectively respond to specific motor outputs and serve as independent computational subunits (Cichon and Gan, 2015). However, other studies suggest that the entire apical tuft acts as a single, independent computational subunit (Xu *et al.*, 2012; Hill *et al.*, 2013; Ujfalussy *et al.*, 2018). Events described as local dendritically-generated spikes were reported in layer II/III neurons of the visual and somatosensory cortex during sensory

stimulation (Smith *et al.*, 2013; Palmer *et al.*, 2014). In the visual cortex, these results suggested that dendritic spikes triggered by visual input enhance somatic tuning to the preferred orientation (Smith *et al.*, 2013). However, single dendrite recordings prevented conclusions about the spatial extent and the branch-specific nature of the detected events. Other studies reported dendritic calcium spikes in association with backpropagating action potentials during spontaneous activity in the motor cortex (Hill *et al.*, 2013) and sensory stimulation in somatosensory cortex (Svoboda *et al.*, 1997; Helmchen *et al.*, 1999; Kerlin *et al.*, 2018). So far however, the recruitment of local and global dendritic events and their coupling with somatic output, remains largely unexplored in awake behaving animals.

In this study, we used multiplane, two-photon calcium imaging to semi-simultaneously monitor calcium transients in different compartments of individual layer 5 pyramidal neurons in the primary visual cortex (V1) of head-fixed awake behaving mice. We imaged calcium signals in the soma, trunk and distal tuft dendrites, both in darkness and during the presentation of drifting gratings, while the animal was either running or stationary. In agreement with a recently published article (Beaulieu-Laroche *et al.*, 2019), we found that the apical trunk dendritic activity was highly correlated with somatic activity. We extend these results, by showing that the whole apical tuft was highly correlated to trunk activity: the vast majority of dendritic calcium transients in the apical tuft were coincident with global events, with rare cases of branch-specific activity, limited to the smallest amplitude events. In addition, we found that somato-dendritic coupling was asymmetric: while almost all events observed in the tuft were also visible in the soma, around 40% of somatic events attenuated in an amplitude and distance-dependent manner from the soma to the apical tuft. Finally, our results show that neither visual stimulation nor locomotion affected the coupling between somatic and apical tuft dendritic calcium signals.

Results

Highly correlated, widespread calcium signals in apical tuft dendrites of single layer 5 neurons

We imaged changes in fluorescence overtime in apical dendrites of individual layer 5 pyramidal neurons sparsely labelled with the calcium sensor GCamP6f (Chen *et al.*, 2013) in the primary visual cortex of adult mice. Using single-plane two-photon imaging (at 120 Hz),

we monitored changes of GCamP6f signals in individual apical tuft dendrites of head-fixed awake behaving mice that were free to run on a cylindrical treadmill (Figure 1A). Our results showed highly correlated calcium signals in all apical branches belonging to the same neuron and imaged in a given field of view (Pearson's correlation coefficient ρ =0.92, SEM = 0.01, n = 25 fields of view recorded from 14 neurons, 6 animals) (Figure 1D). Because distal dendrites are thinner, more excitable and more compartmentalised than proximal tuft dendrites, we tested whether the correlation of calcium transients between apical tuft branches decreased with distance from the apical trunk (nexus). We reconstructed each individual neuron for which we imaged the apical tuft and quantified the correlation of fluorescence signals across sibling branches. We found that calcium signals in sibling branches were highly correlated (average Pearson's correlation coefficient ρ = 0.92) regardless of their branching order (One-way ANOVA, p = 0.34) (Figure 1E,F). Using semi-simultaneous imaging of dendrites at different focal planes within the apical tuft of individual layer 5 neurons, we also found highly correlated calcium signals between proximal and distal tuft branches (average Pearson's correlation coefficient ρ=0.88, Figure 2D(i)). In addition to the global, widespread calcium transients, we also observed in individual spines, independent calcium signals that were not correlated with dendritic signals (Figure 1- figure supplement 1), indicating that in our experimental conditions, we could resolve independent local calcium signals.

We then assessed whether this widespread, highly correlated apical tuft activity was modulated by visual stimulation and locomotion. We found that both visual stimulation and locomotion increased calcium activity in the apical tuft of layer 5 neurons (average ΔF/F0; repeated measure Two-way ANOVA, p = 0.005, 0.003 and 0.99 for visual stimulation, locomotion and interaction between both conditions, respectively; n = 14 neurons) (Figure 1H). However, the high correlation of calcium signals between all imaged dendritic branches was not significantly different between periods of darkness and visual stimulation (drifting gratings) and between stationary and locomotion periods (Two-way ANOVA, p = 0.43, 0.62 and 0.97 for visual stimulation, locomotion and interaction between both conditions, respectively). Finally, we found that the selectivity of the responses to the drifting gratings orientation, quantified by an orientation selectivity index, also did not affect the high correlation of calcium transients in apical tuft dendrites (Figure 1- figure supplement 3).

In line with these findings, we found that branch-specific activity in the apical tuft was rare. We quantified the amount of branch-specific activity in all pairs of branches belonging

125 to the same neuron as the proportion of calcium transients present in one branch and absent
126 in the other pair's branch. Among the 70 imaged branches across 14 neurons, branch-
127 specific calcium transients represented less than 3% of the total number of transients. Among
128 all imaged calcium transients, these local signals were dominated by calcium transients of the
129 smallest amplitudes (Figure 1J). In addition, neither visual stimulation with drifting gratings
130 nor locomotion significantly affected this small proportion of branch-specific calcium signals
131 (Three-way ANOVA, $p < 10^{-15}$ for event amplitude and $p = 0.29$; 0.8 and 0.94, for visual
132 stimulation, locomotion and interaction between both conditions, respectively. No other
133 interaction effect was statistically significant) (Figure 1J). We tested the robustness of our
134 quantification by using different thresholds for the detection of individual calcium transients
135 (Figure 1- figure supplement 2). We found that varying the threshold did not change our
136 findings: the number of branch-specific events ranged between 0.8 and 3.8% and remained
137 limited to transients of the smallest amplitudes (Figure 1- figure supplement 2).
138 Altogether, our results show that apical dendritic calcium signals in V1 layer 5 neurons
139 are almost exclusively dominated by highly correlated calcium transients in the whole apical
140 tuft regardless of the dendritic branching order. Neither visual stimulation nor locomotion
141 modulated this high correlation of apical tuft dendritic calcium signals.
142

143 Calcium signals are highly correlated throughout all compartments of 144 individual layer 5 neurons

145 We then assessed whether the global, widespread apical tuft calcium signals were coupled
146 with somatic activity. For this, we semi-simultaneously imaged GCamP6s calcium signals at
147 two focal planes, separated on average by 170 µm in depth, in 4 different pairs of neuronal
148 compartments from the soma to the apical tuft: Soma-Trunk, proximal Trunk-distal Trunk,
149 distal Trunk-apical Tuft, proximal Tuft-distal Tuft (Figure 2A,B). We used GCamP6s that has
150 higher signal amplitude and signal to noise ratio than GCamP6f in order to increase the
151 detection of somatic signals (Chen *et al.*, 2013). We found that calcium transients
152 simultaneously imaged in each pair of proximal and distal compartments were highly
153 correlated (Figure 2C,D). Since the rise and decay kinetics were slower in somatic signals than
154 in dendritic ones, we performed our quantification on isolated transients (see Methods). For
155 each pair of compartments, we found that the average Pearson's correlation value between

156 the amplitudes of individual transients was 0.88 between the proximal and distal parts of the
157 apical tuft, 0.92 between the trunk and the apical tuft and 0.85 between the proximal and
158 distal trunk. The lowest correlation value was found between the soma and the proximal
159 trunk (0.74, Figure 2D). For each pair of neuronal compartments, shuffling the calcium
160 transients in one compartment resulted in an average correlation value of zero (Figure 2D).
161 Altogether, these results show that calcium transients amplitudes were highly correlated
162 from the soma to the apical tuft of V1 individual layer 5 neurons.
163

164 Frequency of calcium transients decreases in a distance- and amplitude 165 dependent manner from soma to apical tuft

166 We then tested whether the high correlation of calcium transients' amplitudes between soma
167 and apical tuft was associated with distance-dependent changes in the frequency of these
168 events.

169 We quantified the frequency of calcium events in each pair of proximal and distal
170 compartments imaged semi-simultaneously (Figure 3A). We found that the frequency of
171 calcium transients decreased from proximal to distal compartments (Paired t-test, $p = 1.1e^{-6}$,
172 n = 31 pairs of compartments from 19 neurons) by an average of 14% from soma to proximal
173 trunk, 8% from proximal to distal trunk, 24% from distal trunk to apical tuft and 22% form
174 proximal tuft to distal tuft. These proportions indicate a decrease of about 40% of calcium
175 transients from soma to the distal part of the apical tuft (Figure 3B and Figure 3- figure
176 supplement 1). This result was confirmed by a second data set, in which somatic and apical
177 tuft calcium transients were imaged independently (at 120 Hz) in individual layer 5 neurons.
178 We found that the mean frequency of calcium transients in the apical tuft corresponded to
179 62% of the frequency of events in the corresponding soma (Figure 3- figure supplement 1).

180 We then checked whether this decrease in frequency depended on the amplitude of
181 the calcium transients. We calculated the percentage of compartment-specific calcium
182 transients as a function of their amplitude (Figure 3C). The vast majority of compartment-
183 specific events were dominated by calcium transients in proximal compartments that were
184 not detected in distal ones (red trace in figure 3C), while only few calcium transients were
185 found in distal compartments and not in the corresponding proximal one (blue trace in Figure
186 3C) (see also Supplementary video 1 and 2). In addition, our results show that smaller

amplitude calcium transients in the proximal compartment were more likely to attenuate below detection level in the distal compartment compared to larger amplitudes events (red trace in figure 3C). As a result, compartment-specific events were dominated by small amplitude calcium transients in proximal compartments (Two-way ANOVA, $p < 10^{-15}$, $p < 10^{-15}$, $p < 10^{-15}$, for compartment (proximal vs distal), amplitude, and interaction effect, respectively. Figure 4A). Our results were robust to the threshold we used for detecting calcium transients (Figure 1- figure supplement 2). When decreasing the threshold for events detection to up to 30% in the distal compartment, we still observed an amplitude-dependent decay of calcium events in the proximal compartment (Figure 1- figure supplement 2). Similarly, when increasing the threshold by 30% for event detection in the proximal compartment, almost all the events observed distally were also found proximally (Figure 1- figure supplement 2). Due to the scattering nature of cortical tissue, signal to noise ratio decreased with imaging depth. As a consequence, the distance-dependent decrease in frequency may be underestimated.

These results indicate that almost all distal events were found in proximal compartments. Additionally, these findings show that, at least 40% of somatic calcium transients attenuate in a distance dependent manner along the apical trunk and distal dendrites.

Visual stimulation and locomotion do not alter the coupling between soma and apical tuft calcium signals.

We then tested whether visual stimulation and locomotion altered the coupling between the different compartments of individual layer 5 neurons. For each condition, we plotted the percentage of compartment-specific calcium transients as a function of their amplitude and found no significant difference between stationary and locomotion periods and between darkness and visual stimulation (Two-way ANOVA, $p = 0.57$ and $p = 0.14$ for visual stimulation and locomotion, respectively, Figure 4B).

Even though smaller events were attenuated with similar probabilities across the four conditions, calcium transients that do propagate through different neuronal compartments, may be amplified or attenuated in a condition-dependent manner (Figure 4C). To capture these nonlinearities, we plotted the amplitude of each detected transient in each

compartment and calculated a residual value as the distance from the linear robust regression fit (Figure 4C). We then plotted the cumulative distribution of the residual value for every calcium transient in all 4 pairs of imaged compartments from soma to apical tuft. We found that, on average, the non-linear changes in calcium transients' amplitude across neuronal compartments were not significantly different between darkness and visual stimulation nor between stationary and locomotion periods (Paired t-test p = 0.62 and 0.96 respectively, n = 31 pairs of compartments from 19 neurons, Figure 4D).

These results indicate that the coupling between somatic and apical tuft dendritic calcium signals remains unaltered by visual stimulation and locomotion under our experimental conditions.

Discussion

Our results show highly correlated calcium transients in all imaged dendrites of the apical tuft of individual layer 5 neurons in the primary visual cortex of awake behaving mice: we found that branch-specific calcium transients were rare and limited to small amplitude transients. Calcium transients were found to be highly correlated throughout all compartments of individual neurons (soma, trunk, tuft). However, their frequency was found to decrease in a distance- and amplitude-dependent manner from soma to apical tuft. Whereas almost all transients observed in the tuft were present in proximal compartments, the frequency of calcium transients in apical tuft was about 60% of their frequency in the corresponding soma. This indicates that a substantial fraction (40%) of somatic calcium signals attenuate toward the apical tuft. Neither visual stimulation nor locomotion altered the coupling between soma and apical tuft nor the proportion of branch-specific events.

Limitations of the use of calcium imaging to assess dendritic activity in awake behaving mice

Investigations of local dendritic activity in awake behaving mice have so far mainly relied on the use of genetically-encoded calcium indicators (Xu *et al.*, 2012; Cichon and Gan, 2015; Manita *et al.*, 2015; Takahashi *et al.*, 2016; Sheffield, Adoff and Dombeck, 2017; Kerlin *et al.*, 2018; Ranganathan *et al.*, 2018; Sheffield and Dombeck, 2019). The analysis of our data set showed that several experimental constraints may mistakenly bias results towards signals

interpreted as local dendritic activity. Dense labelling was already demonstrated to strongly affect correlation values (Xu *et al.*, 2012); even in cases of relatively sparse labelling of individual neurons, contamination from axons or dendrites of other labelled neurons may lead to local signals detected in single dendrites. In our data set, we systematically reconstructed our imaged neurons and excluded regions of interest where overlapping dendrites from other neurons were observed. Movement artefacts may also lead to inaccurate detection of local dendrite signals; these artefacts are more likely to be found during specific behaviour, such as locomotion, and therefore can bias the interpretation of the results. In our data set we used the activity-independent marker tdTomato to correct for motion artefacts and excluded the recordings in which tdTomato marker was not detected. For most of our imaged neurons, baseline fluorescence of GCamP6 could also be used for the same purpose. Another parameter that may cause artefactual local dendritic signals, is the length of the imaged dendritic segments (and therefore the size of the regions of interest used to extract the changes of fluorescence over time). Small regions of interest could include spines not clearly distinguishable from the corresponding dendritic shaft, especially when the spine is located above the dendrite at the imaged focal plane. As a consequence, in small regions of interests, spine signals may be wrongly interpreted as local dendritic signals.

An additional source of bias is linked to the properties of calcium indicators. Differences in calcium buffering properties of individual compartments lead to different decay times of fluorescent calcium indicators between somatic and dendritic compartments (Kerlin *et al.*, 2018; Beaulieu-Laroche *et al.*, 2019). In order to account for this difference, we based our analysis on the detection of peak amplitudes of individual calcium transients. This detection depends on arbitrary thresholds: we thus showed the robustness of our results across different detection thresholds (Figure 1- figure supplement 2). Finally, our results may be biased by the affinity of GCamP6s. Studies that combined *in vivo* dendritic electrophysiology with calcium imaging have shown that dendritic calcium spikes can reliably be detected with calcium indicators of lower sensitivity than GCamP6f and GCamP6s (Helmchen *et al.*, 1999; Xu *et al.*, 2012). However, while it was shown that GCamP6 could detect individual action potentials in layer 2/3 neurons *in vivo* (Chen *et al.*, 2013), this is not the case for GCamP6f in layer 5 neurons (Beaulieu-Laroche *et al.*, 2019). These results suggest that in our conditions, the detection of somatic action potentials in layer 5 neurons, may be

biased towards larger events, and as a consequence, the attenuation from soma to tuft may be underestimated.

Widespread, correlated calcium transients in apical tuft dendritic branches of layer 5 neurons

Our results show that in the apical tuft, calcium transients were highly correlated regardless of how distal the imaged branches were from the nexus. Branch-specific calcium transients were rare and limited to transients of the smallest amplitudes. These findings suggest that either branch-specific calcium activity is virtually absent and that the entire apical tuft behaves as a single computational unit, or that branch-specific activity is systematically coincident with global tuft calcium events and thus could not be detected with the temporal resolution of GCamP6f. In addition, these results indicate that active dendritic integration in the apical tuft is widely recruited across different behavioural and sensory conditions, not supporting the view of a selective and sparse activity of apical tuft dendrites. Widespread calcium activity throughout the layer 5 apical tuft may strongly influence plasticity and learning (Magee and Johnston, 1997; Golding, Staff and Spruston, 2002; Kampa, Letzkus and Stuart, 2006; Sjöström and Häusser, 2006; Remy and Spruston, 2007; Bittner *et al.*, 2017; Bono and Clopath, 2017; Guerguiev, Lillicrap and Richards, 2017).

Distance dependent attenuation of calcium signals from soma to apical tuft

Our results show an asymmetry in the coupling between somatic and apical tuft calcium signals. Previous studies have shown that dendritic signals attenuate in a distance-dependent manner, suggesting that at least some of the calcium events generated in one compartment would fully attenuate as they reach the next compartment (Stuart, Schiller and Sakmann, 1997; Svoboda *et al.*, 1997; Helmchen *et al.*, 1999; Vetter, Roth and Häusser, 2001; Larkum *et al.*, 2009). To estimate the lower bound proportion of calcium events generated in the tuft and in the soma, we investigated the proportion of attenuated events in both centrifugal and centripetal directions. Our results show that while around 40% of somatic calcium transients decay by the time they reach the apical tuft, only 1.4% of apical tuft calcium events were not associated with somatic events (Figure 4A). These results indicate that at least 40% of somatic calcium transients were not triggered by apical tuft calcium events, and that these transients

311 attenuated from the soma to the apical tuft, suggesting that these calcium transients are
312 associated with back-propagating somatic action potentials. A recent study reported a high
313 somato-dendritic coupling in V1 layer 5 neurons concluding that GCamP6f events occurred
314 concurrently in soma and dendritic compartments without attenuation from soma to apical
315 tuft (Beaulieu-Laroche *et al.*, 2019). This discrepancy may be explained by differences in
316 imaging conditions including a sparse labelling, which reduces the amount of background
317 signals, and the use of GCaMP6s which has a higher signal amplitude and signal to noise ratio
318 than GCamP6f indicator, leading to a higher probability of detecting small events in layer 5
319 somata.

320 The remaining 60% of somatic calcium signals were highly correlated with global apical
321 tuft calcium signals. This result is consistent with two possible mechanisms: either global
322 apical tuft activation systematically triggers somatic action potentials, or global tuft calcium
323 transients are triggered by back-propagating action potentials alone or in conjunction with
324 tuft synaptic inputs. The distance-dependent decrease in the frequency of calcium transients
325 from soma to apical tuft, suggests that at least some of the transients detected in the tuft
326 correspond to calcium signals associated with back-propagating action potentials. Local
327 synaptic inputs in the tuft may then modulate calcium signals triggered by back-propagating
328 action potentials and facilitate further somatic action potentials firing, consistent with
329 Backpropagation-activated calcium spike (BAC) theory (Larkum, 2013; Manita *et al.*, 2015).
330 Alternatively, apical tuft global calcium signals may be generated by tuft synaptic inputs (Xu
331 *et al.*, 2012; Grienberger, Chen and Konnerth, 2015). Further experiments are needed to
332 resolve these mechanisms, for example using voltage-sensitive dyes (Chavarha *et al.*, 2018;
333 Roome and Kuhn, 2018; Adam *et al.*, 2019) or dendritic electrophysiological recordings
334 (Moore *et al.*, 2017), that would provide the temporal resolution to resolve the different types
335 of dendritic events.

336

337 Integration of visual and locomotion-related inputs in layer 5 neurons in awake 338 behaving mice

339 The prevalence and the dynamics of synaptic inputs received by layer 5 pyramidal neurons
340 strongly vary between *in vitro* and *in vivo* conditions, between anesthetized and awake
341 animals and between passive sensory stimulation and active learning tasks (Xu *et al.*, 2012;

342 Hong *et al.*, 2018). It is known that *in vivo*, apical tuft dendrites of layer 5 neurons receive a
343 barrage of thousands of synaptic inputs (Stuart and Spruston, 2015). In awake behaving mice,
344 apical tuft dendrites of V1 layer 5 neurons receive synaptic inputs conveying information
345 about external stimuli (visual stimuli) as well as information about internal variables
346 (arousal/attention, motor activity, predictive signals) (Pakan, Francioni and Rochefort, 2018).
347 Our results show that, in our passive viewing conditions, changes in visual inputs (darkness
348 versus drifting gratings) and locomotion-related inputs do not affect the relationship between
349 somatic and apical tuft calcium signals nor the prevalence of branch-specific dendritic events.
350 It is however possible that during the active learning of a behavioural task, the synaptic
351 inputs associated with this learning process would lead to different mechanisms of dendritic
352 integration than during passive viewing. For example, dendritic integration of multiplicative
353 combinations of sensory and motor inputs in the tuft dendrites of layer 5 pyramidal neurons
354 has been described during an active sensing task in mouse somatosensory cortex
355 (Ranganathan *et al.*, 2018). In addition, it was proposed that changes in neuronal
356 representations during learning would rely on active dendritic signals generating calcium
357 plateau potentials (Bittner *et al.*, 2015; Grienberger *et al.*, 2017). In that case, somato-
358 dendritic coupling may change during the course of learning (Sheffield, Adoff and Dombeck,
359 2017). This remains to be tested in the visual cortex. Similarly, somato-dendritic coupling may
360 evolve during postnatal development when sensori-motor associations are formed. Recently,
361 it was shown in the mouse primary visual cortex, that dendrites of layer 2/3 neurons increase
362 their coupling during adulthood, as a consequence of decreased responsiveness of dendrite-
363 targeting interneurons to locomotion-related inputs (Yaeger, Ringach and Trachtenberg,
364 2019). Further investigations are needed to reveal these mechanisms in layer 5 visual cortical
365 neurons.
366

367 **Materials and Method**

368 **Animals**

369 All experiments and procedures involving animals were approved by the University of
370 Edinburgh Animal Welfare and the ethical review board (AWERB) and performed under the
371 appropriate PIL and PPL license from the UK Home Office in accordance with the Animal

372 (Scientific Procedures) act 1986 and the European Directive 86/609/EEC on the protection of
373 animals used for experimental purposes.
374 Adult males and females aged between 8 and 10 weeks obtained from Jackson Laboratory,
375 ME, USA (B6.Cg-Gt(ROSA)26Sor$^{tm14(CAG-tdTomato)Hze}$/J [RRID:IMSR_JAX:007914]) were used for
376 experiments. Animals were group caged in groups of 2-6 animals, with a running wheel on a
377 reverse 12:12 hour light: dark cycle. They were allowed ad libitum access to food and water.

378 Surgical procedures

379 Viral delivery of GCaMP6

380 To obtain sparse labelling of excitatory neurons we used a cre-dependent approach.
381 AAV1.CamKII.GCaMP6f.WPRE.hGH (Penn Vector core, catalogue No. V4673MI-R) was diluted
382 1:10000 – 1:20000 while either AAV1.Syn.Flex.GCaMP6f.WPRE.SV40 (Penn Vector Core,
383 catalogue No. CS0215) or AAV1.Syn.Flex.GCaMP6s.WPRE.SV40 (Penn Vector Core, catalogue
384 No. CS0408) were diluted 1:10 in the final solution. All dilutions were made in ACSF sterilized
385 using a 0.2 µm syringe filter. AAV1.Syn.Flex.GCaMP6f.WPRE.SV40 was used for experiments
386 in the apical tuft and for non-simultaneous recordings of somatic and dendritic activity, while
387 AAV1.Syn.Flex.GCaMP6s.WPRE.SV40 was used for semi-simultaneous two-planes imaging.

388 Animals were anaesthetized by inhalation of 4% Isoflurane and maintained anaesthetised
389 using 1-2% isoflurane. The animal's body temperature was maintained at physiological levels
390 using a closed-loop, adjustable heating pad monitoring the animal's temperature via a rectal
391 probe. Eye cream (Bepanthen, Bayer) was applied to protect the eyes from dryness and light
392 exposure.

393 After induction of anaesthesia, mice were shaved, mounted onto a stereotaxic frame
394 (David Kopf instruments, CA, USA) and head-fixed using ear bars. An analgesic was
395 administered subcutaneously (Vetergesic, buprenorphine, 0.1 mg/kg of body weight). Layer
396 5 was targeted stereotactically. Injections were performed on the left hemisphere of the brain
397 using a glass pipette (20 µm tip diameter. Nanoject, Drummond Scientific), backfilled with the
398 viral preparation, using a nanoject II (Drummond Scientific), at 2 different depths, 650 and
399 500 µm from brain surface. A total volume of 55.2 nl was injected across the two sites (6x 4.6
400 nl at each location). Single 4.6 nl injections were spaced 30s from one another to allow

401 sufficient time for diffusion. After each injection, pipettes were left in situ for an additional
402 5 min to prevent backflow. The scalp was then sutured (Ethicon, Ethilon polyamide size 6) and
403 the animal monitored during recovery in a heated cage before returning to its home cage for
404 2-3 weeks.

405 Headplate and imaging window

406 Under anaesthesia (isoflurane), mice were shaved, mounted onto a stereotaxic frame (David
407 Kopf instruments, CA, USA) and head-fixed using ear bars. Analgesic and anti-inflammatory
408 drugs were administered subcutaneously (Vetergesic, buprenorphine, 0.1 mg/kg of body
409 weight; Carpaphen, Carprieve, 5mg/kg of body weight; Dexamethasone, Rapidexon, 2mg/kg
410 of body weight). For a cranial window over V1, a section of scalp was removed, the underlying
411 bone was cleansed before a rectangular craniotomy of ~ 2x1.5 mm was made over the left
412 primary visual cortex. The dura was kept intact. The craniotomy was then sealed with a glass
413 cover slip and fixed with cyanoacrylate glue. To stabilize the brain during imaging, we used a
414 triple glass window by stacking three cover-slip glasses (Menzel-Glaser 24x32 mm # 0) on top
415 of each other. These were glued together using an optically clear UV-cured glue (Norland
416 Optical adhesive). Overall, the thickness of the glass window inserted through the cranial
417 window, was comparable to the thickness of the skull at the time of imaging (Smith *et al.*,
418 2017).
419 A custom-built metal headplate was fixed on top of the skull with glue and cemented with
420 dental acrylic (Paladur, Heraeus Kulzer). At the end of the procedure, a single dose of 25ml/kg
421 of Ringer's solution was injected subcutaneously to rehydrate the animal after the procedure.
422 The animal was then released from the head fixation and returned to a heated recovery cage,
423 until full motor capacity was recovered.

424 *In vivo* two-photon imaging data acquisition

425 Imaging was performed using a 25x Objective (Olympus). The excitation wavelength of the
426 laser was set to 920 nm. Layer 5 pyramidal neurons were recorded between 500 and 650 µm
427 below the brain surface and followed up to their distal tuft dendrites along the apical trunk.
428 Neurons which had their nucleus filled with GCaMP6 or had blobby-looking dendrites were
429 excluded for recording. At the end of each imaging session, a z-stack was acquired to allow a

more detailed, offline morphological reconstruction of the imaged neuron. Reconstructions were done using the ImageJ plugin Simple Neurite Tracer. Imaging was performed using a 570 nm short-pass dichroic mirror and two single-band pass filters, a 525/50 (Scientifica) for GCaMP6 light absorption, and a 620/60 (Scientifica) for TdTomato absorption.

Habituation and imaging started 2–3 weeks after AAV injection. Mice were habituated to head-fixation in the dark for 45 min and began to run freely on a polystyrene cylinder (20 cm diameter, on a ball-bearing mounted axis). The mice's running speed on the circular treadmill was continuously monitored using an optical encoder (E7P, 250cpr, Pewatron, Switzerland) connected to a data acquisition device (National Instrument, UK) with custom-written software in LabView (National Instrument, UK) and analysed in MATLAB (Mathworks, MA)

Single-plane two-photon imaging data were acquired using a custom-built galvo-resonant scanning system with a Ti:Sapphire pulsing laser (Chameleon Vision-S, Coherent, CA, USA; < 70 fs pulse width, 80 MHz repetition rate) at 120 Hz, with a custom-programmed LabVIEW-based software (version 8.2; National Instruments, UK). Multi-plane data were acquired using an ultra-fast, solid-state, single 100 fs pulse width laser (InSight DeepSee, SpectraPhysiscs, CA, USA) and a FemtoSmart Dual two-photon microscope (Femtonics, Budapest, Hungary). Two focal planes (512x165 pixels), with an average distance of 170 µm in Z, were imaged at a frequency of 96 frames/s (48 frames/s per plane) using a Piezo objective positioner kit (P725.4CA, Physic Instruments, Germany), switching between planes at 9.6 Hz (4.8 Hz per plane).

Visual stimulation

Visual stimuli were generated using the Psychophysics Toolbox package (Brainard, 1997) for MATLAB (Mathworks, MA) and displayed on a custom-modified backlit LED monitor (51 × 29 cm, Dell, UK) placed 20 cm from the right eye, covering 104° × 72° of the visual field. Visual stimulation trials consisted of drifting full-field square-wave gratings for 3 seconds (spatial frequency of 0.05 cycles per degree, 1.5 Hz, 8 equally spaced directions in randomized order, contrast 80%, mean luminance 37 cd/m^2). Drifting gratings were separated from one another by 4 seconds of isoluminant grey periods. Time stamps for the onset of every stimulus were recorded and aligned to imaging frames using custom-built Matlab scripts.

461

462 **Data Analysis**

463 Image analysis and signal extraction

464 To correct for brain motion after image acquisition, we used 2D plane translation-based image
465 alignment (SIMA 1.2.0, sequential image analysis; Kaifosh et al., 2014). We 3D reconstructed
466 each imaged neuron and defined regions of interest (ROIs) corresponding to neuronal cell
467 body and dendritic segments manually. Due to sparse labelling, signal contamination was
468 negligible in most cases. In cases ROIs were contaminated by labelled structures from other
469 neurons, we excluded those ROIs from further analysis.
470 The pixel intensity within each ROI was averaged to create a raw fluorescence time series F(t).
471 Baseline fluorescence F0 was computed for each neuron by taking the fifth percentile of the
472 smoothed F(t) (1 Hz lowpass, zero-phase, 60th-order FIR filter) over each trial (F0(t)),
473 averaged across all trials. As a consequence, the same baseline F0 was used for computing
474 the changes in fluorescence in darkness and during visual stimulation. The change in
475 fluorescence relative to baseline, ΔF/F0 was computed by taking the difference between F
476 and F0(t) and dividing by F0.
477 Single plane data was acquired at 120 Hz, and subsequently downsampled to 5Hz for
478 signal processing. Multi-plane data were analysed at 4.8 Hz.
479

480 Calcium transients analysis

481 We first estimated noise levels by filtering our ΔF/F0 signal using a 9th order, zero-phase, high-
482 pass filter at 0.6 Hz (Matlab function *filter*). We then estimated the standard deviation of the
483 filtered signal and used a threshold of 2.8 of this standard deviation to detect individual
484 calcium transients, using the built-in Matlab function *findpeaks.* We tested the robustness of
485 our results to different thresholds +/- 30% of the selected threshold (Figure 1- figure
486 supplement 2). For each peak found in any branch or compartment, we defined an event as
487 coincident in another branch or compartment when it occurred in a time window of 3 seconds
488 around the frame where the first peak was originally detected (2 seconds before, 1 after).
489 99% of coincident events were observed within +/- 0.73 ms. Each event could only be

490 considered coincident with one event. The amplitude of a calcium event was determined by
491 taking the difference between the ΔF/F0 amplitude at the frame in which a peak was detected
492 and a local minimum in a 2 seconds, backward sliding window. Correlation values were
493 calculated as the Pearson's correlation values between event amplitudes in pairs of branches
494 or compartments. Shuffling values were obtained by randomly shuffling the order of the
495 events in one branch or compartment of each pair analysed. Residuals were extracted by
496 calculating the robust linear regression line between normalised event amplitudes in two
497 compartments, and then extracting the distance, along the y-axis, of each individual point
498 from this robust line.

499

500 Locomotion analysis

501 Changes in the position of the cylindrical treadmill (sampled at 12,000 Hz) were interpolated
502 to match the rate of imaging. To define stationary and locomotion periods we used the
503 following criteria: Stationary corresponded to periods where the instantaneous speed (as
504 measured at the 40 Hz sampling rate) was less than 0.1 cm/s. Locomotion corresponded to
505 periods meeting three criteria: instantaneous speed ≥ 0.1 cm/s, 0.25 Hz lowpass filtered
506 speed ≥ 0.1 cm/s, and an average speed ≥ 0.1 cm/s over a 2 s window cantered at this point
507 in time. Any inter-locomotion interval shorter than 500 ms was also labelled as locomotion.
508 Stationary periods less than 3 s after or 0.2 s before a period of locomotion were removed
509 from the analysis.

510 Orientation Selectivity

511 The orientation selectivity index (OSI) was calculated as $(O_{pref}-O_{orth})/(O_{pref}-O_{orth})$ where O_{pref}
512 represents the mean ΔF/F0 value during the presentation of the preferred orientation across
513 trials and O_{orth} represents the mean ΔF/F0 value at the orthogonal orientation compared to
514 preferred. The preferred stimulus of each neuron was the orientation that elicited the
515 maximal response when averaged across all trials.

516 **Statistics**

517 All analysis was performed either in Matlab 2017a, or in GraphPad Prism 8. All error bars in
518 the figures represent standard error of the mean. The details of the statistical test we used,

as well the details about what we used as independent samples can be found in the relevant figure legends.

Acknowledgments

We thank the GENIE Program and the Janelia Research Campus, specifically V. Jayaraman, R. Kerr, D. Kim, L. Looger, and K. Svoboda, for making GCaMP6 available. This work was funded by the Wellcome Trust and the Royal Society (Sir Henry Dale fellowship to N.R.), the Marie Curie Actions of the European Union's FP7 program (MC-CIG 631770 to N.R.), the Shirley Foundation, the Patrick Wild Center and the RS MacDonald Charitable Trust Seedcorn Grant (to N.R.), the Simons Initiative for the Developing Brain (to N.R.) and the University of Edinburgh (PhD scholarship to V.F.).

Declaration of Interests

The authors declare no competing interests

References

Adam, Y. *et al.* (2019) 'Voltage imaging and optogenetics reveal behaviour- dependent changes in hippocampal dynamics', *Nature*. Springer US. doi: 10.1038/s41586-019-1166-7.

Beaulieu-Laroche, L. *et al.* (2019) 'Widespread and Highly Correlated Somato-dendritic Activity in Cortical Layer 5 Neurons', *Neuron*. Elsevier Inc., pp. 1–7. doi: 10.1016/j.neuron.2019.05.014.

Bittner, K. C. *et al.* (2015) 'Conjunctive input processing drives feature selectivity in hippocampal CA1 neurons', *Nature Neuroscience*, 18(8), pp. 1133–1142. doi: 10.1038/nn.4062.

Bittner, K. C. *et al.* (2017) 'Behavioral time scale synaptic plasticity underlies CA1 place fields', *Science*, 357(6355), pp. 1033–1036. doi: 10.1126/science.aan3846.

Bono, J. and Clopath, C. (2017) 'Modeling somatic and dendritic spike mediated plasticity at the single neuron and network level', *Nature Communications*. Springer US, 8(1), p. 706. doi: 10.1038/s41467-017-00740-z.

Chavarha, M. *et al.* (2018) 'Fast two-photon volumetric imaging of an improved voltage

549 indicator reveals electrical activity in deeply located neurons in the awake brain', *BioRXiv*.

550 Chen, T.-W. *et al.* (2013) 'Ultrasensitive fluorescent proteins for imaging neuronal activity.',
551 *Nature*, 499(7458), pp. 295–300. doi: 10.1038/nature12354.

552 Cichon, J. and Gan, W.-B. (2015) 'Branch-specific dendritic Ca2+ spikes cause persistent
553 synaptic plasticity', *Nature*, 520(7546), pp. 180–185. doi: 10.1038/nature14251.

554 Dadarlat, M. C. and Stryker, M. P. (2017) 'Locomotion Enhances Neural Encoding of Visual
555 Stimuli in Mouse V1', *The Journal of Neuroscience*, 37(14), pp. 3764–3775. doi:
556 10.1523/JNEUROSCI.2728-16.2017.

557 Dipoppa, M. *et al.* (2018) 'Vision and Locomotion Shape the Interactions between Neuron
558 Types in Mouse Visual Cortex.', *Neuron*. doi: 10.1016/j.neuron.2018.03.037.

559 Erisken, S. *et al.* (2014) 'Effects of Locomotion Extend throughout the Mouse Early Visual
560 System', *Current Biology*. Elsevier Ltd, 24(24), pp. 1–9. doi: 10.1016/j.cub.2014.10.045.

561 Golding, N. L., Staff, N. P. and Spruston, N. (2002) 'Dendritic spikes as a mechanism for
562 cooperative long-term potentiation', *Nature*, 418(6895), pp. 326–331. doi:
563 10.1038/nature00854.

564 Grienberger, C. *et al.* (2017) 'Inhibitory suppression of heterogeneously tuned excitation
565 enhances spatial coding in CA1 place cells', *Nature Neuroscience*, 20(3), pp. 417–426. doi:
566 10.1038/nn.4486.

567 Grienberger, C., Chen, X. and Konnerth, A. (2015) 'Dendritic function in vivo', *Trends in*
568 *Neurosciences*. Elsevier Ltd, 38(1), pp. 45–54. doi: 10.1016/j.tins.2014.11.002.

569 Guerguiev, J., Lillicrap, T. P. and Richards, B. A. (2017) 'Towards deep learning with segregated
570 dendrites', *eLife*, 6, pp. 1–37. doi: 10.7554/eLife.22901.

571 Harris, K. D. and Shepherd, G. M. G. (2015) 'The neocortical circuit: themes and variations',
572 *Nature Neuroscience*, 18(2), pp. 170–181. doi: 10.1038/nn.3917.

573 Helmchen, F. *et al.* (1999) 'In vivo dendritic calcium dynamics in deep-layer cortical pyramidal
574 neurons', *Nature Neuroscience*. doi: 10.1038/14788.

575 Hill, D. N. *et al.* (2013) 'Multibranch activity in basal and tuft dendrites during firing of layer 5
576 cortical neurons in vivo', *Proceedings of the National Academy of Sciences*, 110(33), pp.
577 13618–13623. doi: 10.1073/pnas.1312599110.

578 Hong, Y. K. *et al.* (2018) 'Sensation, movement and learning in the absence of barrel cortex',
579 *Nature*. Springer US, pp. 542–546. doi: 10.1038/s41586-018-0527-y.

580 Jaffe, D. B. *et al.* (1992) 'The spread of Na+ spikes determines the pattern of dendritic Ca2+
581 entry into hippocampal neurons', *Nature*, 357(6375), pp. 244–246. doi: 10.1038/357244a0.

582 Kampa, B. M., Letzkus, J. J. and Stuart, G. J. (2006) 'Requirement of dendritic calcium spikes
583 for induction of spike-timing-dependent synaptic plasticity', *The Journal of Physiology*, 574(1),

pp. 283–290. doi: 10.1113/jphysiol.2006.111062.

Kerlin, A. *et al.* (2018) 'Functional clustering of dendritic activity during decision-making', *bioRxiv*. doi: 10.1101/440396.

Kim, E. J. *et al.* (2015) 'Three Types of Cortical Layer 5 Neurons That Differ in Brain-wide Connectivity and Function', *Neuron*. Elsevier Inc., 88(6), pp. 1253–1267. doi: 10.1016/j.neuron.2015.11.002.

Larkum, M. (2013) 'A cellular mechanism for cortical associations: An organizing principle for the cerebral cortex', *Trends in Neurosciences*. Elsevier Ltd, 36(3), pp. 141–151. doi: 10.1016/j.tins.2012.11.006.

Larkum, M. E. *et al.* (2009) 'Synaptic integration in tuft dendrites of layer 5 pyramidal neurons: A new unifying principle', *Science*, 325(5941), pp. 756–760. doi: 10.1126/science.1171958.

Larkum, M. E., Zhu, J. J. and Sakmann, B. (1999) 'A new cellular mechanism for coupling inputs arriving at different cortical layers', *Nature*. doi: 10.1038/18686.

Magee, J. C. and Johnston, D. (1997) 'A synaptically controlled, associative signal for Hebbian plasticity in hippocampal neurons', *Science*. doi: 10.1126/science.275.5297.209.

Manita, S. *et al.* (2015) 'A Top-Down Cortical Circuit for Accurate Sensory Perception', *Neuron*. Elsevier Inc., 86(5), pp. 1304–1316. doi: 10.1016/j.neuron.2015.05.006.

Moore, J. J. *et al.* (2017) 'Dynamics of cortical dendritic membrane potential and spikes in freely behaving rats', *Science*, 355(6331), p. eaaj1497. doi: 10.1126/science.aaj1497.

Pakan, J. M., Francioni, V. and Rochefort, N. L. (2018) 'Action and learning shape the activity of neuronal circuits in the visual cortex', *Current Opinion in Neurobiology*, 52, pp. 88–97. doi: 10.1016/j.conb.2018.04.020.

Palmer, L. M. *et al.* (2014) 'NMDA spikes enhance action potential generation during sensory input', *Nature Neuroscience*. Nature Publishing Group, 17(3), pp. 383–390. doi: 10.1038/nn.3646.

Ramaswamy, S. and Markram, H. (2015) 'Anatomy and physiology of the thick-tufted layer 5 pyramidal neuron', *Frontiers in Cellular Neuroscience*, 9(June), pp. 1–29. doi: 10.3389/fncel.2015.00233.

Ranganathan, G. N. *et al.* (2018) 'Active dendritic integration and mixed neocortical network representations during an adaptive sensing behavior', *Nature Neuroscience*. Springer US. doi: 10.1038/s41593-018-0254-6.

Remy, S. and Spruston, N. (2007) 'Dendritic spikes induce single-burst long-term potentiation', *Proceedings of the National Academy of Sciences*, 104(43), pp. 17192–17197. doi: 10.1073/pnas.0707919104.

Roome, C. J. and Kuhn, B. (2018) 'Simultaneous dendritic voltage and calcium imaging and somatic recording from Purkinje neurons in awake mice', *Nature Communications*. Springer

US, 9(1), p. 3388. doi: 10.1038/s41467-018-05900-3.

Schiller, J. *et al.* (1997) 'Calcium action potentials restricted to distal apical dendrites of rat neocortical pyramidal neurons', *The Journal of Physiology*, 505(3), pp. 605–616. doi: 10.1111/j.1469-7793.1997.605ba.x.

Sheffield, M. E. and Dombeck, D. A. (2019) 'Dendritic mechanisms of hippocampal place field formation', *Current Opinion in Neurobiology*. Elsevier Ltd, 54, pp. 1–11. doi: 10.1016/j.conb.2018.07.004.

Sheffield, M. E. J., Adoff, M. D. and Dombeck, D. A. (2017) 'Increased Prevalence of Calcium Transients across the Dendritic Arbor during Place Field Formation', *Neuron*. Elsevier Inc., 96(2), pp. 490-504.e5. doi: 10.1016/j.neuron.2017.09.029.

Sjöström, P. J. and Häusser, M. (2006) 'A Cooperative Switch Determines the Sign of Synaptic Plasticity in Distal Dendrites of Neocortical Pyramidal Neurons', *Neuron*, 51(2), pp. 227–238. doi: 10.1016/j.neuron.2006.06.017.

Smith, I. T. *et al.* (2017) 'Stream-dependent development of higher visual cortical areas', *Nature Neuroscience*, 20(2), pp. 200–208. doi: 10.1038/nn.4469.

Smith, S. L. *et al.* (2013) 'Dendritic spikes enhance stimulus selectivity in cortical neurons in vivo', *Nature*, 503(7474), pp. 115–120. doi: 10.1038/nature12600.

Spruston, N. *et al.* (1995) 'Activity-dependent action potential invasion and calcium influx into hippocampal CA1 dendrites', *Science*, 268(5208), pp. 297–300. doi: 10.1126/science.7716524.

Stuart, G. J. and Spruston, N. (2015) 'Dendritic integration: 60 years of progress', *Nature Neuroscience*, 18(12), pp. 1713–1721. doi: 10.1038/nn.4157.

Stuart, G., Schiller, J. and Sakmann, B. (1997) 'Action potential initiation and propagation in rat neocortical pyramidal neurons', *The Journal of Physiology*, 505(3), pp. 617–632. doi: 10.1111/j.1469-7793.1997.617ba.x.

Svoboda, K. *et al.* (1997) 'In vivo dendritic calcium dynamics in neocortical pyramidal neurons', *Nature*, 385(6612), pp. 161–165. doi: 10.1038/385161a0.

Takahashi, N. *et al.* (2016) 'Active cortical dendrites modulate perception', *Science*, 354(6319), pp. 1587–1590. doi: 10.1126/science.aah6066.

Ujfalussy, B. B. *et al.* (2018) 'Global and Multiplexed Dendritic Computations under In Vivo-like Conditions', *Neuron*. doi: 10.1016/j.neuron.2018.08.032.

Vetter, P., Roth, A. and Häusser, M. (2001) 'Propagation of Action Potentials in Dendrites Depends on Dendritic Morphology', *Journal of Neurophysiology*, 85(2), pp. 926–937. doi: 10.1152/jn.2001.85.2.926.

Waters, J. *et al.* (2003) 'Supralinear Ca 2+ Influx into Dendritic Tufts of Layer 2/3 Neocortical Pyramidal Neurons In Vitro and In Vivo', *The Journal of Neuroscience*, 23(24), pp. 8558–8567.

doi: 10.1523/JNEUROSCI.23-24-08558.2003.

Xu, N. *et al.* (2012) 'Nonlinear dendritic integration of sensory and motor input during an active sensing task.', *Nature*. Nature Publishing Group, 492(7428), pp. 247–51. doi: 10.1038/nature11601.

Yaeger, C. E., Ringach, D. L. and Trachtenberg, J. T. (2019) 'Neuromodulatory control of localized dendritic spiking in critical period cortex', *Nature*. Springer US, pp. 100–104. doi: 10.1038/s41586-019-0963-3.

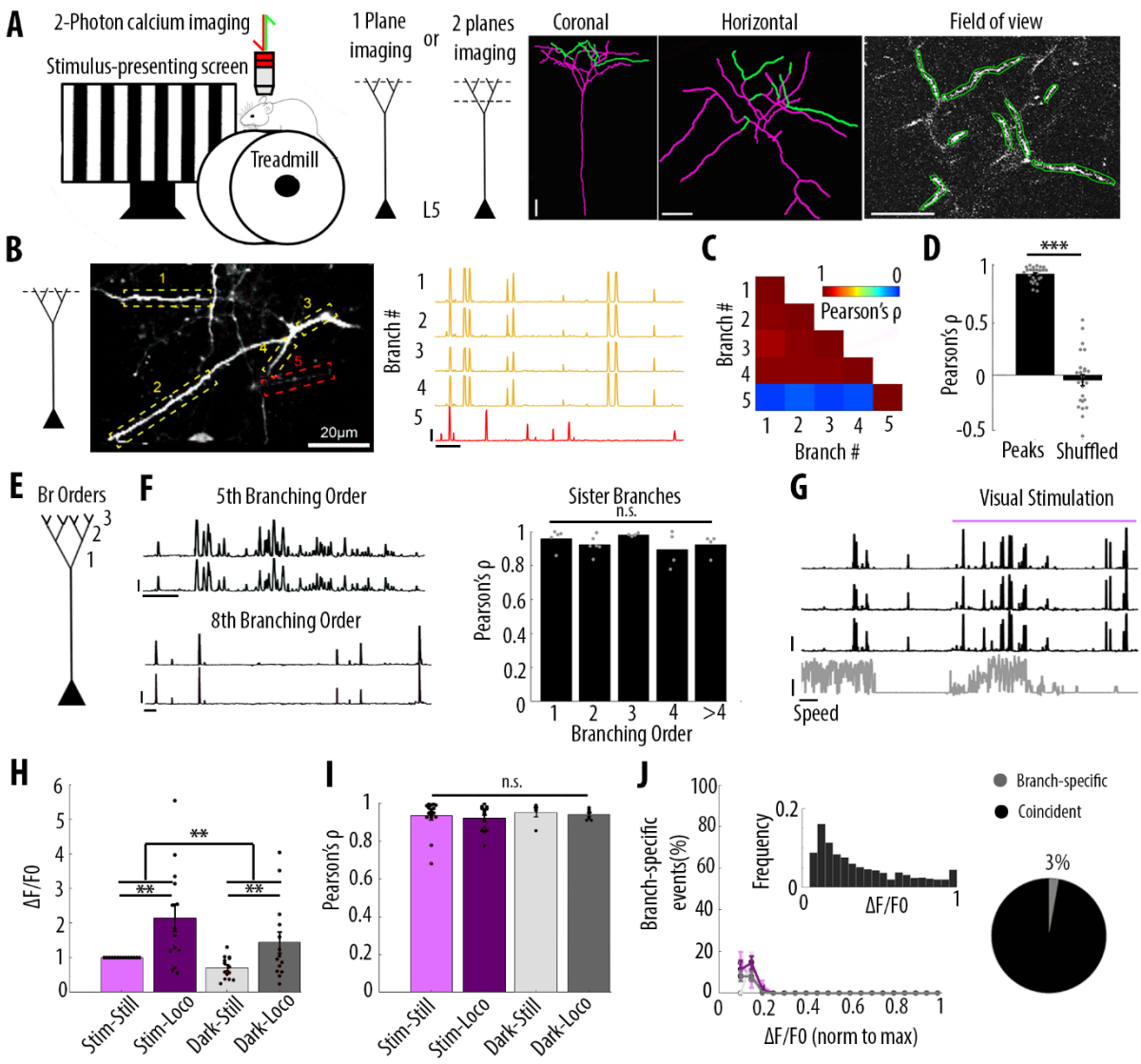

Figure 1. Highly correlated activity in the whole apical tuft of layer 5 pyramidal neurons. **A**) Schematic of the methodological approach. Calcium transients were recorded either in multiple apical tuft dendrites in a single focal plane, or semi-simultaneously in different compartments of the neuron (Soma, Trunk and Tuft). At the end of each imaging session, a z-stack was recorded for post-hoc reconstruction of each imaged neuron. **B**) Single plane imaging of the apical tuft branches of an individual layer 5 neuron. Calcium transients of the apical tuft branches belonging to one neuron are shown in yellow and calcium transients of tuft branch belonging to a different neuron is shown in red. Scale bars, 0.3 ΔF/F0 (normalised to max), 20 s. **C**) Pearson's correlation matrix between the calcium activity of the branches shown in B. Branches that belong to the same neuron (neuron 1) have a mean Pearson's correlation of 0.96, while the branch that belongs to the different neuron (neuron 2) has a mean Pearson's

correlation value of 0.13 with neuron 1's branches. **D**) Mean Pearson's correlation value ρ for each imaged field of view and corresponding shuffled data (Paired t-test, $p = 3.5e^{-15}$; n = 25 field of view; coming from 14 neurons; 6 animals; 70 branches). **E**) Schematic of our definition of branching orders. **F**) Two representative traces of sibling branches belonging to the 5th and 8th (left panel, labelled) branching order and a quantification of the Pearson's correlation ρ for sibling tuft branches of different branching orders (right panel). (For 1st, 2nd, 3rd, 4th and more than 4th branching order, One-way ANOVA, p = 0.34; n = 5; 6; 4; 4; 4 pairs of branches, respectively). Scale bars, 0.3 ΔF/F0 (normalised to max), 20 s. **G**) Representative traces of 3 tuft branches belonging to the same neuron while the animal was either stationary or locomoting (lower panel) during either darkness or the presentation of drifting grating (purple segment). Scale bars, 12 cm/s, 0.3ΔF/F0 (normalised to max), 20 s. **H**) Mean ΔF/F0 for apical tuft dendrites during darkness and visual stimulation while the animal was either stationary of locomoting. Bar graph is normalised to visual stimulation during stationary condition. Both visual stimulation and locomotion significantly increase the mean ΔF/F0 of tuft branches without any interaction effect (Repeated Measures Two-way ANOVA on log-transformed data, p = 0.0053, 0.0026 and 0.99 for the visual stimulation, locomotion and interaction effects respectively, n = 14 neurons). **I**) Pearson's correlation coefficients ρ for the apical tuft branches of individual neurons during the four conditions (stim and stationary, stim and loco, dark and stationary, dark and loco). (Two-way ANOVA, p = 0.43, 0.62 and 0.97 for visual stimulation, locomotion and interaction effects; n =16; 14; 5 and 7 field of views respectively). **J**) Weighted mean of the proportion of branch-specific events as a function of event's amplitude for the four different conditions (lower left panel). Neither visual stimulation nor locomotion nor an interaction effect, increased the number of branch specific events (Three-way ANOVA, p = 0.29; 0.8 and 0.94, respectively; $p < 10^{-15}$ for event amplitude). *Upper left panel*, frequency distribution of the events' amplitudes detected in the apical tuft branches. *Right panel*, pie chart showing that on average 3% of the total events were detected in only one branch.

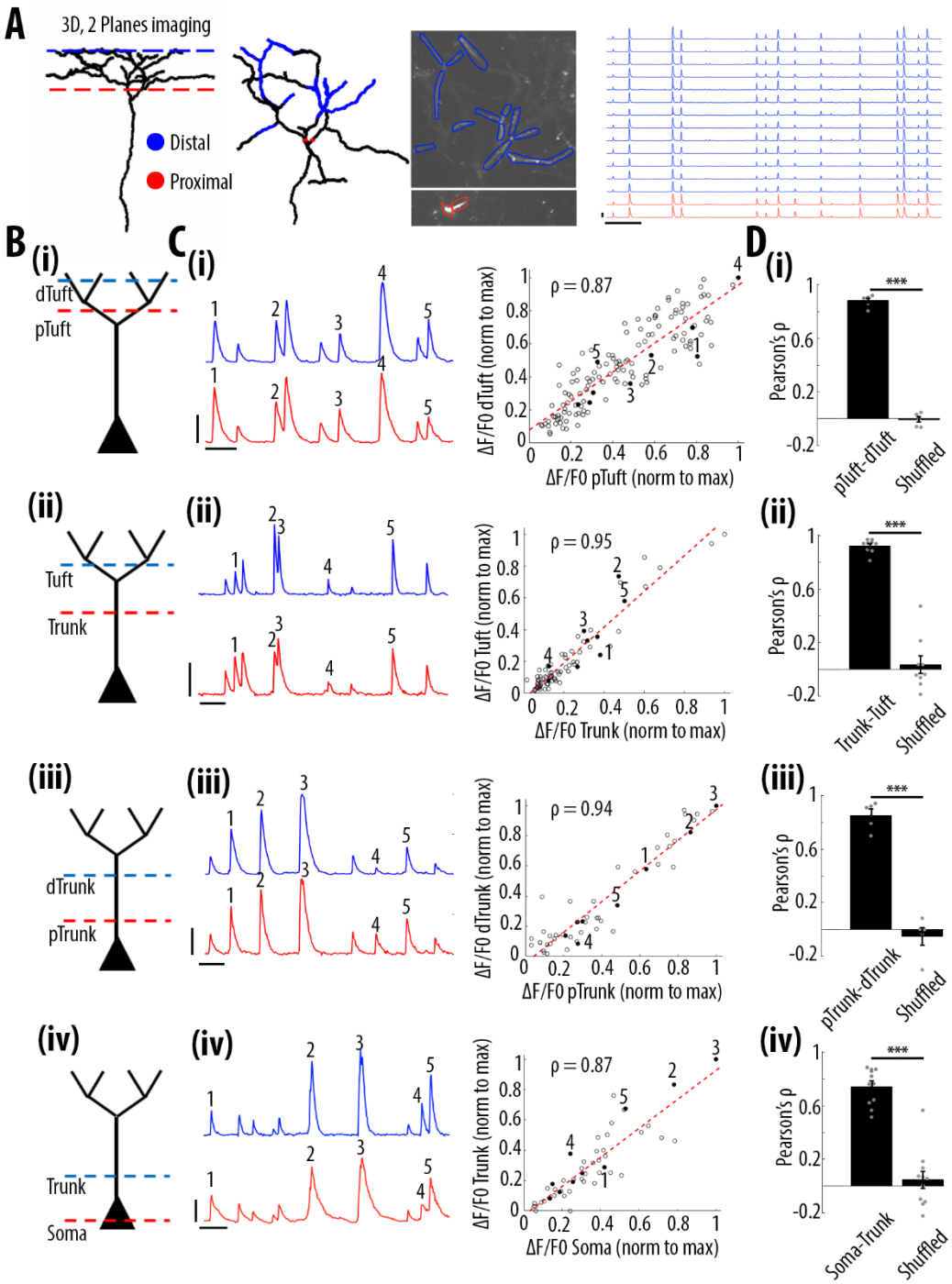

Figure 2. High correlation of calcium transients from soma to apical tuft dendrites of individual layer 5 neurons. A) Morphological reconstruction of a neuron imaged at two focal planes semi-simultaneously. *Left panel*, coronal view of the imaged neuron. Red and blue dotted lines indicate the planes of imaging. *Middle left panel*, horizontal view of the same neuron. Branches highlighted in red and blue, represent the same dendritic branches observed in the middle right panel. *Right panel*, each trace represents the calcium activity of an individual branch shown in the middle panels. **B**) Schemata of the compartments imaged simultaneously,

712 (i) tuft-tuft, (ii) trunk-tuft, (iii), trunk-trunk, (iv) soma-trunk. pTrunk, dTrunk and pTuft, dTuft
713 indicate proximal and distal portions of the trunk and the apical tuft, respectively. **C**) *Left panel*,
714 representative calcium events recorded in two neuronal compartments semi-simultaneously as
715 shown in B. *Right panel*, scatter plot showing the correlation of the amplitude of calcium
716 transients in each compartment imaged simultaneously, and shown in B. Each dot represents a
717 calcium transient. Filled dots are the same transients shown in the left panel and indicated by
718 numbers. Scale bars 0.3 $\Delta F/F0$ (normalised to max), 10 s. **D**) Pearson's correlation values ρ for
719 each pair of compartments imaged semi-simultaneously and compared to its corresponding
720 shuffled data (Paired t-test, pTuft-dTuft(i), $p = 1.6e^{-6}$, n = 6 pairs; Trunk-Tuft(ii), $p = 8e^{-7}$, n =
721 9; pTrunk-dTrunk(iii), $p = 4.4e^{-4}$, n = 5; Soma-Trunk(iv), $p = 4.4e^{-6}$, n = 11).

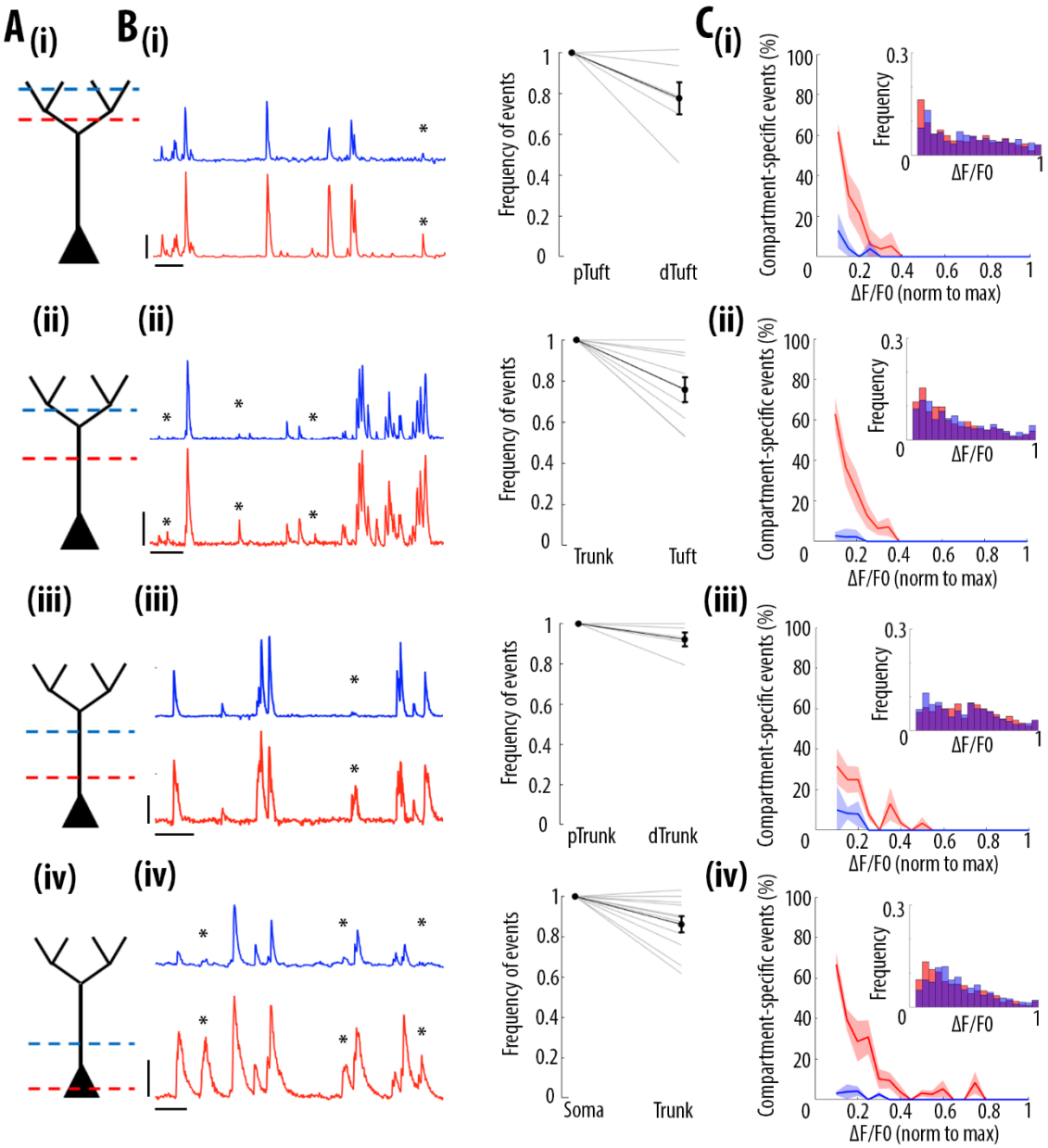

Figure 3. Frequency of calcium transients decreases in a distance and amplitude-dependent dependent manner from the soma to the apical tuft. A) Schemata of the compartments imaged simultaneously. **B**) *Left panel*, representative ΔF/F0 traces of calcium activity recorded semi-simultaneously in two different compartments of individual neurons. Asterisks indicate calcium transients detected in the proximal compartment (red trace) and not detected in the distal one (blue trace). *Right panel*, frequency of detected calcium transients, normalised to the proximal compartment. Individual lines represent individual neurons. Scale bars 0.25 ΔF/F0 (normalised to max), 20 s. **C**) Proportion of compartment-specific events as a function of calcium transients' amplitude. In red, proportion of events detected in the proximal

compartment only. In blue, proportion of events detected in the distal compartment only. *Upper right panel*, in red and blue the frequency histogram of calcium transients amplitudes detected in the proximal and distal compartments, respectively. Thick line represents the weighted mean proportion. Shaded area represents the weighted SEM for each bin (0.05 size). For all compartments, event amplitude, compartment (proximal vs distal) and an interaction between these two factors significantly affected the proportion of compartment-specific events (Two-way ANOVA, pTuft-dTuft (i), $p < 10^{-15}$, $p = 7.8x10^{-5}$, $p = 6.2x10^{-8}$, for event amplitude, proximal versus distal compartment and interaction between amplitude and compartment, respectively, n = 6 pairs; Trunk-Tuft(ii), $p < 10^{-15}$, $p = 3.4x10^{-9}$, $p < 10^{-15}$, n = 9; pTrunk-dTrunk(iii), $p = 1.3x10^{-13}$, $p = 2.4x10^{-4}$, $p = 7x10^{-3}$, n = 5; Soma-Trunk(iv), $p < 10^{-15}$, $p < 10^{-15}$ and $p < 10^{-15}$, n = 11).

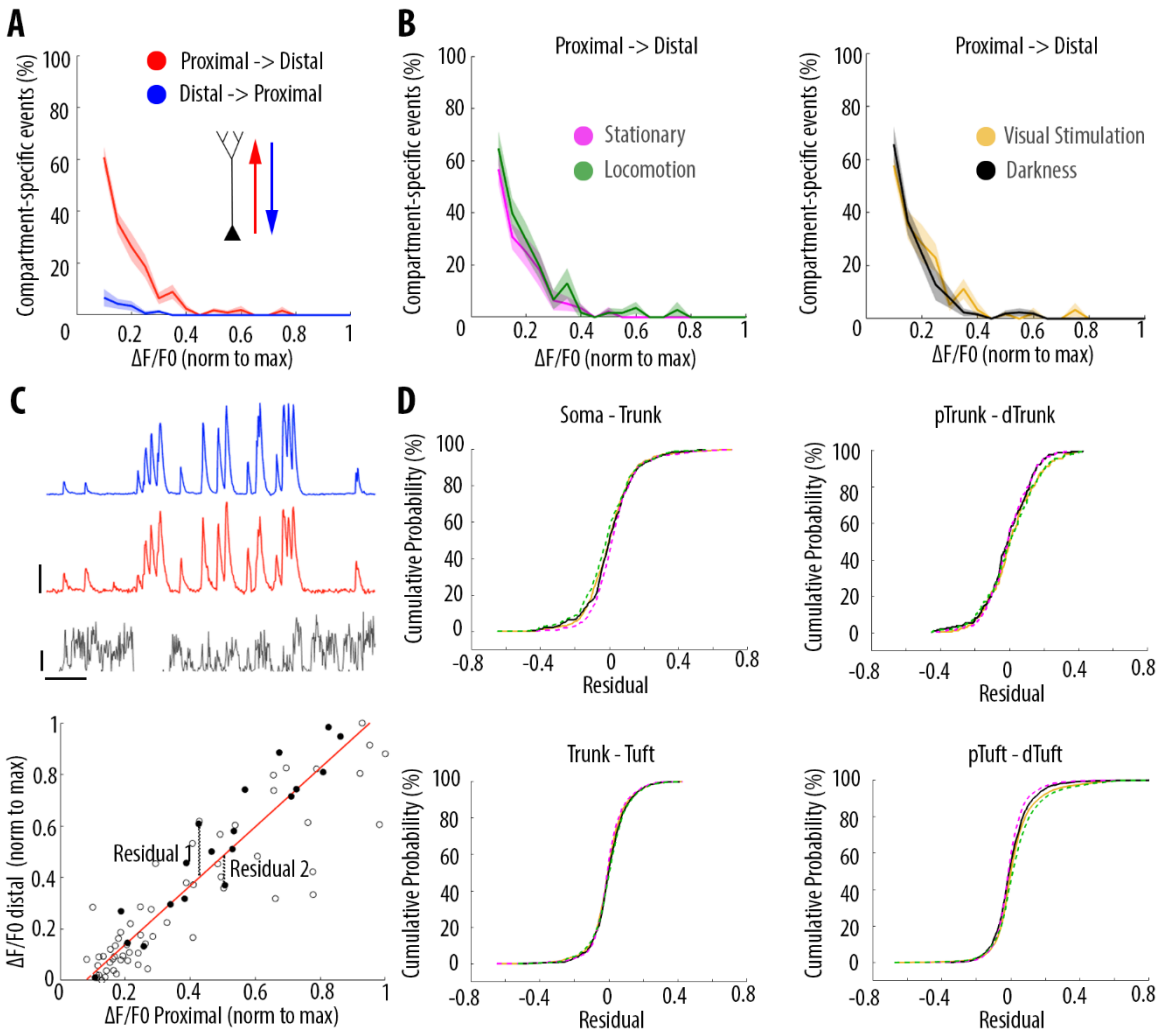

Figure 4. Locomotion and visual stimulation do not alter the relationship between somatic and dendritic activity in individual layer 5 pyramidal neurons. A) Mean proportion of compartment-specific events as a function of calcium transient amplitude. Data points from figure 3C(i-iv) have been averaged together. In red, events found in the proximal, but not in the distal compartment. In blue, events that are found in the distal, but not proximal compartment. Event amplitude, compartment (proximal vs distal) and an interaction between these two factors significantly affected the proportion of compartment-specific events (Two-way ANOVA, $p < 10^{-15}$, $p < 10^{-15}$, $p < 10^{-15}$, n = 31 pairs of compartments from 19 neurons). **B**) Neither visual stimulation nor locomotion alter the curve describing amplitude-dependent decay of events in the proximal-to-distal direction (Two-way ANOVA, p = 0.57 and p = 0.14

for visual stimulation and locomotion, respectively). **C**) *Upper panel*, representative traces of the proximal (red) and distal (blue) compartment imaged semi-simultaneously, during stationary and locomotion periods (lower trace shows speed). Scale bars represent 0.25 ΔF/F0 (normalised to max), 12 cm/s, 20 s. *Lower panel*, scatter plot between the amplitudes of calcium transients for the ΔF/F0 trace shown above. Individual dots represent individual calcium transients. Filled dots are the same as shown in the upper panel. The red line represents the robust linear regression fit. For each transient, a residual from the robust linear regression was calculated. **D**) Cumulative distribution function for the residuals calculated for each pairs of compartments and for each condition. Neither visual stimulation nor locomotion alter the relationship between somatic and dendritic activity in individual layer 5 neurons (Paired t-test for the effect of visual stimulation and locomotion on residuals: Soma-Trunk(iv), $p = 0.33$ and 0.30, respectively, $n = 11$ pairs; pTrunk-dTrunk(iii), $p = 0.34$ and 0.93, $n = 5$; Trunk-Tuft(ii), $p = 0.5$ and 0.95, $n = 9$; pTuft-dTuft(iv), $p = 0.83$ and 0.08, $n = 6$).

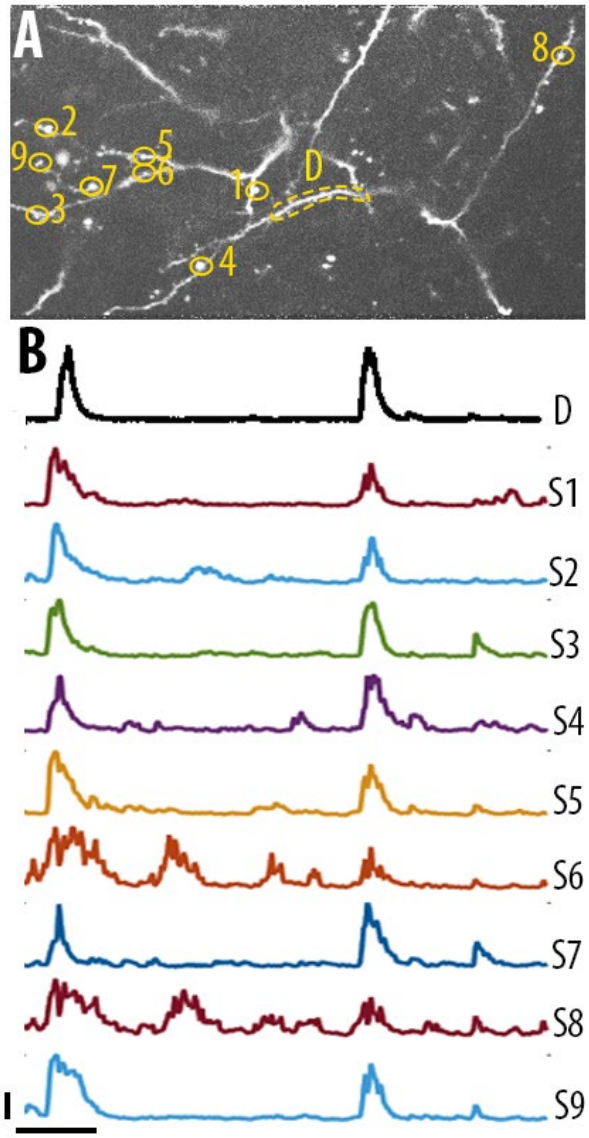

Figure 1- figure supplement 1. Independent single spine activity in the apical tuft dendrites of layer 5 neurons. A) Field of view showing the apical tuft branches of an individual GCamP6-labelled layer 5 neuron. **B**) ΔF/F0 traces for the individual spines shown in A during a single, 65 seconds-long trial. Error bars indicate 0.3 ΔF/F0 (normalised to max), 10 s.

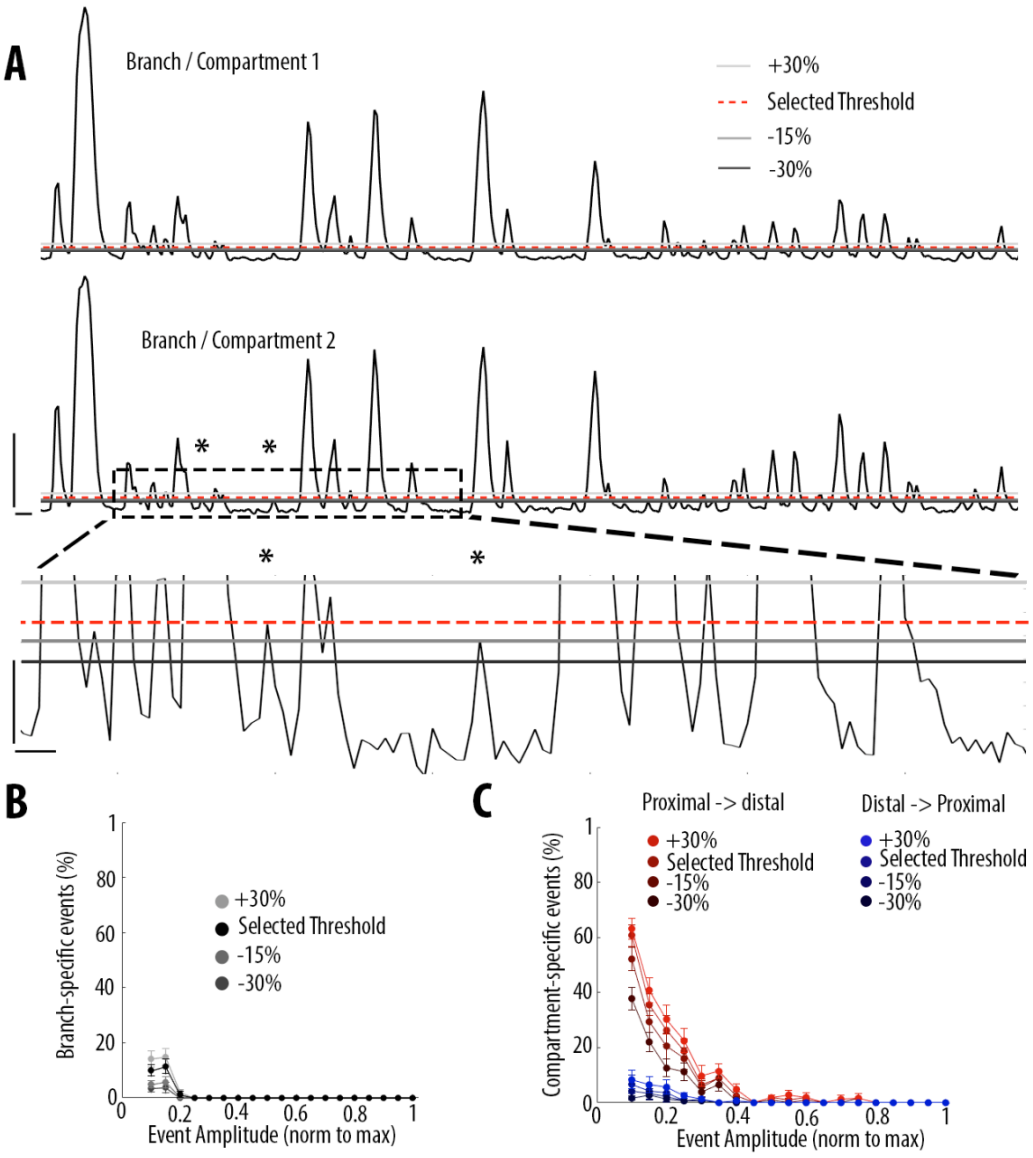

Figure 1- figure supplement 2. Impact of threshold for calcium transients detection. A) To assess the amount of branch / compartment specific events, for every transient detected in one branch / compartment, we assessed whether there was another corresponding event in the second branch / compartment (see Methods). *Upper panel*, ΔF/F0 traces of two sibling branches in the apical tuft branches of a single layer 5 pyramidal neurons. Asterisks indicate two events which were not detected using the selected threshold but were detected lowering the threshold by 30%. *Lower panel*, zoomed image of the dotted area in the upper panel. To assess the resilience of our observed effects to different thresholds, we assessed the amount of branch / compartment specific events, keeping the selected threshold in one branch / compartment (red-dotted line) and varying the threshold in the second branch / compartment from +30% to -30% (light, medium and dark grey lines, respectively). Scale bars: upper panel,

788 0.3 ΔF/F0 (normalised to max), 5 s; lower panel: 0.03 ΔF/F0, 1s. **B**) Number of branch-specific
789 events detected as a function of the amplitude and threshold selected. **C**) Number of
790 compartment-specific events detected as a function of the amplitude and threshold selected.
791

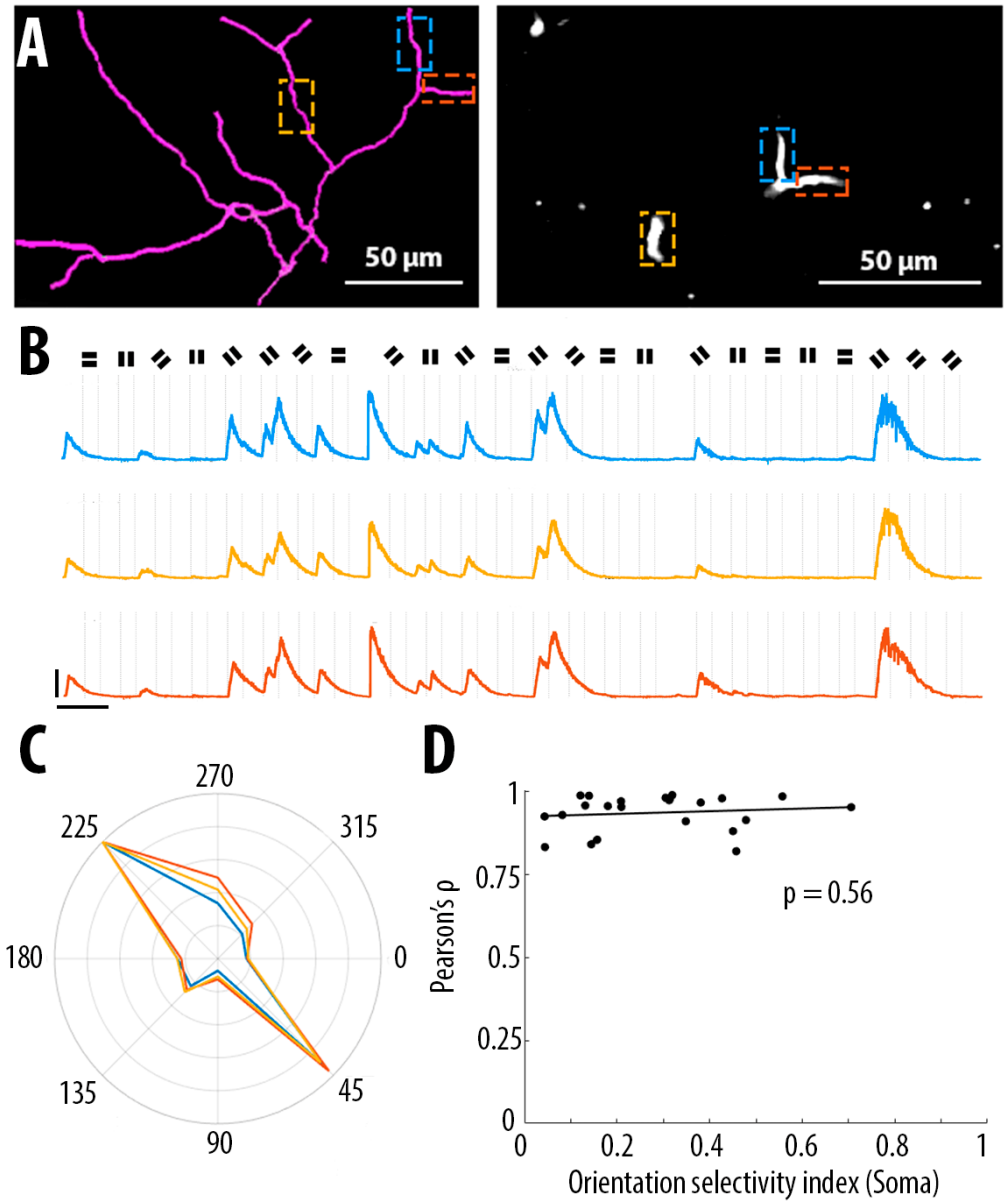

Figure 1- figure supplement 3. High correlation of calcium transients in apical tuft dendrites, independent of somatic orientation selectivity. A) Morphological reconstruction of three apical tuft branches that were imaged during the presentation of eight drifting gratings. **B**) ΔF/F0 traces of the branches shown in A, in response to drifting gratings of four different orientations (3 s gratings interleaved by 4 s isoluminant grey screen). Scale bars 0.3 ΔF/F0 (normalised to max), 10 s. **C**) Polar plot quantifying the responses of these 3 branches to the eight oriented gratings. **D**) Mean Pearson's correlation value ρ of all imaged branches per neuron, as a function of the orientation selectivity of the corresponding soma (each dot represents a neuron; n = 23 neurons). The straight black line represents the best fit.

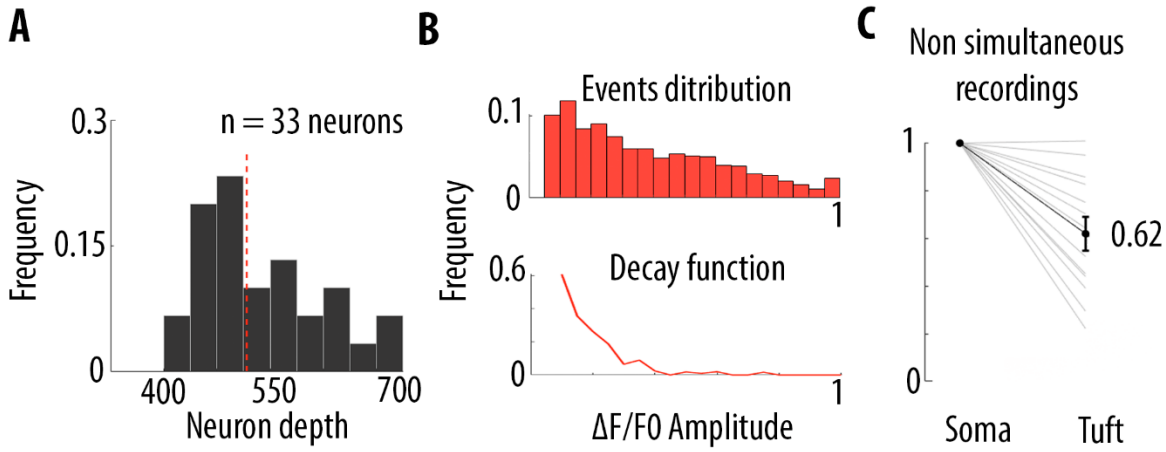

Figure 3- figure supplement 1. Decreased frequency of calcium events from soma to apical tuft. A) Frequency distribution of the depths at which neurons have been imaged. The red dotted line indicates the median (528 µm from the dura). **B**) Calculation of the proportion of somatic events, decaying from the soma to the most distal part of the tuft. Pairs of compartments (soma-trunk, trunk-trunk, trunk-tuft, tuft-tuft) were recorded at a distance of 170 µm (see Methods). As a consequence, the average amplitude-dependent decay function (lower panel, same as figure 4A) represents the decay of calcium transients within 170 µm. To calculate how many events attenuate from the soma to the most distal part of the apical tuft (528 µm apart, on average), we projected the decay measured within 170 µm, to a distance of 528 µm. We multiplied the amplitude-dependent decay function by the scaling factor 3.1 (528/170) and we applied this scaled function to the event distribution (upper panel) at each bin (0.05 ΔF/F0). The event distribution was derived by averaging all the calcium events in all the proximal compartments (see distribution of event amplitudes for each proximal compartment in red in figure 3). Using this approach, we calculated that the proportion of events that decay from the soma to the tuft was 39%, for the data set in which pairs of compartments were imaged semi-simultaneously. **C**) Proportion of events in the tuft, relative to the corresponding soma, for neurons in which both compartments were imaged non-simultaneously.